

Enhancing Thermoelectric Properties Through a Three-Terminal Benzene Molecule

Z. Sartipi¹ and J. Vahedi^{*1,2}

¹*Department of Physics, Sari Branch, Islamic Azad University, Sari, Iran and*

²*Laboratoire de Physique Theorique et Modelisation, CNRS UMR 8089, Universite de Cergy-Pontoise, 95302 Cergy-Pontoise Cedex, France.*

(Dated: May 22, 2018)

The thermoelectric transport through a benzene molecule with three metallic terminals is discussed. Using general local and non-local transport coefficients, we investigated different conductance and thermopower coefficients within the linear response regime. Based on the Onsager coefficients which depend on the number of terminal efficiencies, efficiency at maximum power is also studied. In the three-terminal set up with tuning temperature differences, a great enhancement of the figure of merit is observed. Results also show that the third terminal model can be useful to improve the efficiency at maximum output power compared to the two-terminal model.

PACS numbers: 85.65.+h, 85.80.Fi

I. INTRODUCTION

Thermoelectricity has recently received enormous attention due to the powerful ways of energy conversion. Enhancing the efficiency of thermoelectric materials, in the whole range spanning from macro- to nano-scales, is one of great importance for several different technological applications¹⁻⁴. The efficiency of a thermoelectric device consisting of two terminals is determined by its thermoelectric figure of merit ($ZT = \frac{GS^2}{K}T$), where T is the temperature, S is the Seebeck coefficient (thermopower), G is the electrical conductance, and K is the thermal conductance given by $K = K_p + K_e$ where K_p (K_e) is the phononic (electronic) contribution to K . Clearly, ZT can be increased by enhancing the power factor (S^2GT) or reducing the thermal conductivity and therefore a high-performance thermoelectric material should possess a large thermopower and electrical conductivity and simultaneously a low thermal conductivity. As these factors are correlated, increasing ZT to values greater than unity is challenging. One promising approach has been to reduce the contribution of phonons by nanostructuring materials⁵.

While most of the researches have been conducted in two-terminal setups, transport in multi-terminal devices has begun to be investigated since these more complex designs may offer additional advantages⁶⁻¹⁶. An interesting perspective, for instance, is the possibility to exploit a third terminal in order to decouple the charge and energy flows and improve thermoelectric efficiency¹⁷⁻²⁰.

From an application point of view, the systems with high thermoelectric efficiency would be useful for waste energy harvesting²¹⁻²³. Since the efficiency at maximum power monotonically depends on the thermoelectric figure of merit²⁴, it is important to find heterostructures²⁵⁻²⁸ or bulk materials²⁹, where the large thermopower guarantees high values of ZT . In this regard multi-terminal nanostructures offer enhanced flexibility and therefore it might be useful to improve efficiency^{7,30-32} especially under broken time-reversal symmetry^{11,17,18}. In these structures, the non-

equilibrium conditions are accompanied by significant non-local effects which require proper definitions of transport coefficients. Mazza et al. derived an analytical expression for local and non-local transport coefficients and investigated how a third terminal could improve the performance of a quantum system³⁰. In addition, Mechalek et al. propose an experimental protocol for determination of the transport coefficients in terms of the local and non-local conductances and thermopowers in three-terminal structures with a quantum dot³³. Erdman et al., study the thermoelectric properties and heat-to-work conversion performance of an interacting, multi-level quantum dot (QD) weakly coupled to electronic reservoirs³⁴.

The nanostructuring of materials is also a crucial factor in the improvement of power factor because it can yield sharp features in the electronic density of states and the transmission coefficient which describe the propagation of electrons through a device. Even though these existed works, it is still desirable to explore new low-dimensional thermoelectric materials. In particular, the rapidly growing amount of research in atomic and molecular nanostructures should be notices. In this spirit, the use of single-molecule junctions has become an interesting topic in the field of molecular electronics. They are a powerful tool for detection of the intrinsic physical and chemical properties³⁵⁻⁴³. The charge transport through the single benzene molecular junction has attracted a considerable attention and has become one of the most intensively studied nanoscale systems. Based on the benzene molecular junction, researchers able to manipulate single-molecule devices were in the Coulomb blockade regime⁴¹, observed the quantum interference effect⁴² and studied the thermoelectric effects⁴³ in both experimental and theoretical methods.

We consider a benzene molecule for the central region since this configuration can highlight a series of complex interference effects due to multiple allowed pathways which can lead to Fano-like resonances in the transmission spectrum⁴⁴. Note that quantum effects yielding Fano resonances in the transmission spectra were predicted to have an impact on the thermoelectric efficiency

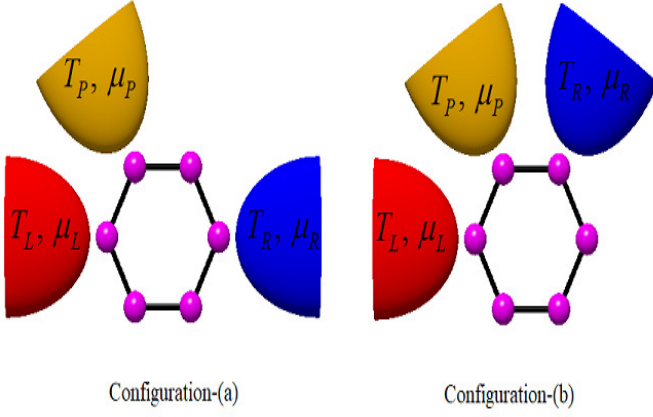


FIG. 1: A schematic view of the benzene molecule coupled to three nonmagnetic leads.

of single molecule devices⁴⁵, nanoscale junctions⁴⁶ and quantum dot systems^{47–49}. In addition to the dramatic effects of quantum interference on the performance of our system as a heat engine, our aim is to investigate how the efficiencies at maximum output power, output power, and figures of merit evolve when the system is driven from a two terminal to a three-terminal configuration.

The rest of the paper is structured as follows: section-II provides theory and formalism. Results are presented in section-III and section-IV gives a summary and conclusion.

II. MODEL, THEORY AND FORMALISM

Fig.1 shows a benzene molecule connected to three nonmagnetic leads, which can be described by the Hamiltonian as follows

$$\mathcal{H} = \mathcal{H}_{leads} + \mathcal{H}_m + \mathcal{H}_{tun}$$

where $\mathcal{H}_{leads} = \sum_{\alpha k} \varepsilon_{\alpha k} c_{\alpha k}^\dagger c_{\alpha k}$ is the Hamiltonian of three ($\alpha = R, P, L$) leads connected to the benzene molecule. $c_{\alpha k}^\dagger$ creates an electron in the $\alpha = L, P, R$ lead with energy ε_k . The Hamiltonian of the benzene molecule is $\mathcal{H}_m = \sum_i \varepsilon_i d_i^\dagger d_i + t \sum_{ij} (d_i^\dagger d_j + h.c)$, where $d_i^\dagger (d_i)$ is the creation (annihilation) operator of an electron at site i in the benzene molecule, ε_i and t describe the on-site energy and the nearest-neighbour hopping integral in the benzene molecule, respectively. The last term is the tunneling between leads and molecule $\mathcal{H}_{tun} = \sum_{\alpha k i} \gamma_{\alpha k i} (c_{\alpha k}^\dagger d_i + h.c)$, where $\gamma_{\alpha k i}$ represents the coupling strength between the molecule and leads. For a scattering region including a benzene molecule in contact with three leads, we can express the transmission probability as $\mathcal{T}(E) = Tr(\Gamma_i G^r \Gamma_j G^a)$, where $\Gamma_\alpha = i(\Sigma_\alpha - \Sigma_\alpha^\dagger)$, ($\alpha = L, P, R$) is the broadening matrix due to the coupling to leads, where Σ_α being the self-energy of lead i .

G^a and G^r are advanced and retarded green function of the molecule, respectively. Note that in the wide band limit approximation, we set $\Sigma_\alpha = -i\frac{\gamma_\alpha}{2}$, where γ_α does not depend on energy. This choice yields the identification $\Gamma_\alpha = \gamma_\alpha$.

A. Non-equilibrium thermodynamics

The system under consideration (see Fig.1) is characterized by three energy and particle currents J_α^U and J_α^N ($\alpha = L, R, P$), respectively, which flow from the corresponding terminals, in accordance with the constraint $\sum_\alpha J_\alpha^{U(N)} = 0$. Note that positive values correspond to flows from the terminals to the system. We will set electrode R as a reference ($(T_R, \mu_R) \equiv (T, \mu)$). To guarantee the linear response regime is considered, we set $(T_\alpha, \mu_\alpha) \equiv (T + \delta T_\alpha, \mu + \delta \mu_\alpha)$ with $|\delta \mu_\alpha|/k_B T \ll 1$ and $|\delta T_\alpha|/T \ll 1$ for $\alpha = L, P$, where k_B is the Boltzmann constant. Two thermodynamic forces $X_{L,P}^\mu$ and $X_{L,P}^T$ and their fluxes $J_{L,P}^N$ and $J_{L,P}^Q$ response can describe the non-equilibrium thermodynamics processes^{51,52}. During the processes, total charge x transfer from one terminal to another one is done by work $W = -Fx$ against an external thermodynamic force F . The corresponding force is $X_{L,P}^\mu = F/T$ which T being the temperature of the system and $F = \delta \mu_{L,P}/e$, where e is the electron charge. The thermodynamic flux is defined as $J_{L,P}^N = dx/dt$. We are interested in the heat to work conversion, that is, the work is performed by converting part of the heat Q which flows from the hot terminals. Regarding the linear regime, the temperature difference $\delta T_{L,P} = T_{L,P} - T$ is small compared to $T_L \approx T_P \approx T_R$, thus the thermodynamic force is $X_{L,P}^T = \delta T_{L,P}/T^2$, and the heat current is $J_{L,P}^Q = dQ/dt$.

For a three-terminal setup, the elements of the Onsager matrix is related to eight quantities (details are presented in Appendix A). The matrix elements can be categorized in two local and non-local thermopower $S_{\alpha\beta}$, the electrical $G_{\alpha\beta}$ and thermal $K_{\alpha\beta}$ conductances. The non-local ($\alpha \neq \beta$) coefficients describe how bias driven between two terminals can influence transport in another terminal. We follow Ref.[30] terminology, so let's define the transport coefficients for a three-terminal system as follows

$$\begin{aligned} S_{LL} &= \frac{1}{eT} \frac{\mathcal{L}_{13;32}^{(2)}}{\mathcal{L}_{13;31}^{(2)}}, & S_{PP} &= \frac{1}{eT} \frac{\mathcal{L}_{14;31}^{(2)}}{\mathcal{L}_{13;31}^{(2)}} \\ S_{LP} &= \frac{1}{eT} \frac{\mathcal{L}_{13;34}^{(2)}}{\mathcal{L}_{13;31}^{(2)}}, & S_{PL} &= \frac{1}{eT} \frac{\mathcal{L}_{13;21}^{(2)}}{\mathcal{L}_{13;31}^{(2)}}. \end{aligned} \quad (1)$$

$$\begin{aligned} G_{LL} &= \frac{e^2 \mathcal{L}_{11}}{T}, & G_{PP} &= \frac{e^2 \mathcal{L}_{33}}{T} \\ G_{LP} &= \frac{e^2 \mathcal{L}_{13}}{T}, & G_{PL} &= \frac{e^2 \mathcal{L}_{13}}{T}. \end{aligned} \quad (2)$$

$$\begin{aligned}
K_{LL} &= \frac{1}{T^2} \frac{\mathcal{L}_{12}L_{12;32}^{(2)} - \mathcal{L}_{12}L_{13;32}^{(2)} - \mathcal{L}_{11}\mathcal{L}_{23;23}^{(2)}}{\mathcal{L}_{13;31}^{(2)}} \\
K_{PP} &= \frac{1}{T^2} \frac{\mathcal{L}_{14}\mathcal{L}_{13;43}^{(2)} - \mathcal{L}_{13}\mathcal{L}_{14;43}^{(2)} - \mathcal{L}_{11}\mathcal{L}_{34;34}^{(2)}}{\mathcal{L}_{13;31}^{(2)}} \\
K_{LP} &= \frac{1}{T^2} \frac{\mathcal{L}_{24}\mathcal{L}_{13;31}^{(2)} - \mathcal{L}_{14}\mathcal{L}_{13;23}^{(2)} - \mathcal{L}_{34}\mathcal{L}_{13;12}^{(2)}}{\mathcal{L}_{13;31}^{(2)}} \\
K_{PL} &= K_{LP} \tag{3}
\end{aligned}$$

where $\mathcal{L}_{ij}^{(2)} = \mathcal{L}_{ik}\mathcal{L}_{lj} - \mathcal{L}_{il}\mathcal{L}_{kj}$. It is worth also that by disconnecting terminal P from the rest, two-terminal well known formula for Seebeck coefficient, electrical and thermal conductance can be recovered as $S_{LL} = \frac{1}{eT} \frac{\mathcal{L}_{12}}{\mathcal{L}_{11}}$, $G_{LL} = \frac{e^2}{T} \mathcal{L}_{11}$ and $K_{LL} = \frac{1}{T^2} \frac{\mathcal{L}_{12;12}^{(2)}}{\mathcal{L}_{11}^{(2)}}$, respectively. The Onsager coefficients \mathcal{L}_{ij} are obtained by the linear response expansion of the currents J_i (see Appendix B).

B. Efficiency at maximum output power

We aim to create a heat engine, so we should consider its efficiency. But we just interested in the efficiency at maximum output power $\eta(\mathbf{P}_{max})$. Indeed, we look for the value of the efficiency at chemical potential which optimizes the output power generated by the heat engine. Thus we first need to define the output power $\mathbf{P} = \frac{dW}{dt}$ where W denotes the work performed by the system against an external force F . This can be recast base on generalized forces and fluxes as $\mathbf{P} = -T(J_L^N X_L^\mu + J_P^N X_P^\mu)$

Having the output power the the steady-state efficiency of the heat engine can be defined as the output power \mathbf{P} , divided by the sum of the heat currents absorbed by the engine $\eta = \frac{\mathbf{P}}{\sum_{\alpha} J_{\alpha}^Q}$, with constrain of positive heat currents in the \sum_{α} in the denominator . Note that the signs of the heat currents depend on the details of the system, thus the efficiency depends on which heat currents are positive. In the three-terminal model considered in this work (see Fig.1), we focus on the situation where J_R^Q is negative. So the efficiency can be defined as $\eta_{LP} = \frac{\mathbf{P}}{J_L^Q + J_P^Q}$ when both J_L^Q and J_P^Q are positive and given as $\eta_{L(P)} = \frac{\mathbf{P}}{J_{L(P)}^Q}$ when either J_L^Q or J_P^Q is

positive³⁰. For the sake of simplicity and without loss of generality, we set $T_L > T_P > T_R$, thus $\delta T_L > \delta T_P > 0$.

The electrochemical forces $X_{L,P}^\mu$ that maximize output power at given temperature forces $X_{L,P}^T$ can be written as

$$\begin{aligned}
X_L^\mu &= \frac{-eT}{2} (S_{LP}X_P^T + S_{LL}X_L^T) \\
X_P^\mu &= \frac{-eT}{2} (S_{PL}X_L^T + S_{PP}X_P^T) \tag{4}
\end{aligned}$$

inserting these expressions into the output power yields

$$\mathbf{P}_{max} = \frac{T^4}{4} (\mathcal{X}^\dagger \mathcal{M} \mathcal{X}) \tag{5}$$

where $\mathcal{X}^\dagger = [X_L^T \ X_P^T]$ and $\mathcal{M} = \begin{bmatrix} \mathcal{M}_{11} & \mathcal{M}_{12} \\ \mathcal{M}_{21} & \mathcal{M}_{22} \end{bmatrix}$ is a positive semi-definite matrix, whose elements are defined as follows,

$$\begin{aligned}
\mathcal{M}_{12} &= \mathcal{M}_{21} = G_{LP}S_{LP}S_{PL} + G_{LP}S_{LL}S_{PP} \\
&\quad + G_{PP}S_{PL}S_{PP} + G_{LL}S_{LL}S_{LP} \\
\mathcal{M}_{11} &= G_{LL}S_{LP}^2 + 2 G_{LP}S_{LP}S_{PP} + G_{PP}S_{PP}^2 \\
\mathcal{M}_{22} &= G_{LL}S_{LL}^2 + 2 G_{LP}S_{PL}S_{LL} + G_{PP}S_{PL}^2 \tag{6}
\end{aligned}$$

inserting \mathcal{M} into \mathbf{P}_{max} gives

$$\mathbf{P}_{max} = \left(\frac{T^4}{4} \right) \mathcal{N}^2 (\lambda_1 \cos^2 \theta + \lambda_2 \sin^2 \theta) \tag{7}$$

where $\mathcal{N} = \|(X_L^T \ X_P^T)\|$ is the system temperature and the angle θ determines the rotation in the $(X_L^T \ X_P^T)$ plane that defines the eigenvectors of \mathcal{M} . Here the parameter $\rho = (\lambda_1 \cos^2 \theta + \lambda_2 \sin^2 \theta)$ has the meaning of power factor for three-terminal system which relates the maximum output power to the temperature differences (for more details we refer interested readers to Ref. [30]).

Now using Eq.(7), one can obtain the efficiency at maximum output power $\eta(\mathbf{P}_{max})$. Analog to the equation of efficiency at maximum power for two-terminal cases, for three the terminal configuration, the efficiency at maximum output power can also be expressed in terms of the Carnot efficiencies³⁰ as follows

$$\begin{aligned}
\eta_L(\mathbf{P}_{max}) &= \frac{\eta_{cL}}{2} \frac{Z_L^{\mathcal{M}_{11}}T + 2\mathcal{K}Z_L^{\mathcal{M}_{12}}T + \mathcal{K}^2Z_L^{\mathcal{M}_{22}}T}{2\mathcal{F}_1 + 4\mathcal{K}\mathcal{F}_1 + 2\mathcal{K}^2 + Z_L^{\mathcal{M}_{11}}T + 2\mathcal{K}Z_L^{\mathcal{M}_{12}}T + \mathcal{K}^2Z_L^{\mathcal{M}_{22}}T} = \frac{\eta_{cL}}{2} \frac{Z_L T}{\mathcal{W}_L + Z_L T} \\
\eta_P(\mathbf{P}_{max}) &= \frac{\eta_{cP}}{2} \frac{Z_P^{\mathcal{M}_{11}}T + 2\mathcal{K}Z_P^{\mathcal{M}_{12}}T + \mathcal{K}^2Z_P^{\mathcal{M}_{22}}T}{2\mathcal{K}^2\mathcal{F}_1 + 4\mathcal{K}\mathcal{F} + 2 + Z_P^{\mathcal{M}_{11}}T + 2\mathcal{K}Z_P^{\mathcal{M}_{12}}T + \mathcal{K}^2Z_P^{\mathcal{M}_{22}}T} = \frac{\eta_{cP}}{2} \frac{Z_P T}{\mathcal{W}_P + Z_P T} \\
\eta_{LP}(\mathbf{P}_{max}) &= \frac{\eta_{cLP}}{2} \frac{Z_{LP}^{\mathcal{M}_{11}}T + 2\mathcal{K}Z_{LP}^{\mathcal{M}_{12}}T + \mathcal{K}^2Z_{LP}^{\mathcal{M}_{22}}T + \mathcal{O}(\delta T)}{2\mathcal{F}^{-1} + 4\mathcal{K} + 2\mathcal{F}^2\mathcal{K}_1^{-1} + Z_{LP}^{\mathcal{M}_{11}}T + 2\mathcal{K}Z_{LP}^{\mathcal{M}_{12}}T + \mathcal{K}^2Z_{LP}^{\mathcal{M}_{22}}T + \mathcal{O}(\delta T)} \simeq \frac{\eta_{cLP}}{2} \frac{Z_{LP} T}{\mathcal{W}_{LP} + Z_{LP} T} \tag{8}
\end{aligned}$$

where the constants, $\mathcal{W}_L=2\frac{\mathcal{F}_1}{\mathcal{F}} + 4\mathcal{K}\mathcal{K}_1 + 2\mathcal{K}^2$, $\mathcal{W}_P=2\mathcal{K}^2\frac{\mathcal{F}}{\mathcal{F}_1} + 4\mathcal{K}\mathcal{F} + 2$ and $\mathcal{W}_{LP}=\mathcal{F}_1^{-1} + \mathcal{K}^2\mathcal{F}^{-1} + 2\mathcal{K}$. η_{cLP} , η_{cP} and η_{cL} are corresponding Carnot efficiencies. One has defined the parameters $\mathcal{K}=\frac{X^T}{X_P^T}$, $\mathcal{F}=\frac{K_{LP}}{K_{PP}}$ and $\mathcal{F}_1=\frac{K_{LP}}{K_{LL}}$. And the combination of the figure of merit

$$\begin{aligned} Z_\alpha T &= (Z_\alpha^{\mathcal{M}_{11}} + 2\mathcal{K}Z_\alpha^{\mathcal{M}_{12}} + \mathcal{K}^2Z_\alpha^{\mathcal{M}_{22}}) T, \quad (\alpha = L, P) \\ Z_{LP} T &= \left(Z_{LP}^{\mathcal{M}_{11}} + 2\mathcal{K}Z_{LP}^{\mathcal{M}_{12}} + \mathcal{K}^2Z_{LP}^{\mathcal{M}_{22}} \right) T \end{aligned} \quad (9)$$

where $Z_\alpha^j T$ ($j=\mathcal{M}_{11}, \mathcal{M}_{12}, \mathcal{M}_{22}$) are generalized figures of merit defined as $Z_L^j T = \frac{j^T}{K_{LL}} T$, $Z_P^j T = \frac{j^T}{K_{PP}}$ and $Z_{LP}^j T = \frac{j^T}{K_{LP}}$. For detailed calculations, we refer readers to Ref. [30].

III. RESULTS AND DISCUSSION

In this section, we present the numerical results. The parameters used are as follows: nearest neighbor hopping energy in the Benzene molecule is set as $t = 1.5eV$, and the coupling are considered constant in the wideband approximation. For temperature setup we use a parameter M which is defined by $\delta T_P = M\delta T_L$. Room temperature $T = 300$ is chosen as the reference temperature.

Results of conductance and Seebeck coefficients as a function of incoming electron energy are plotted in Fig. 2. For comparison purpose, the two terminal model also considered (shown in blue line). Two cases of local and non-local coefficients are labeled with $A_{\alpha\alpha}$ and $A_{\alpha\beta}$, respectively, where $A = G, S$ and $\alpha, \beta = L, R, P$. We should also note that the results depicted in Fig. 2 are based on the configuration-(a) (see Fig. 1) and we fix $M = 0.1$. It can be seen that for the two-terminal case, the electrical conductance (blue line) shows four resonance peaks located at $\varepsilon = \pm 1.5eV$ and $\varepsilon = \pm 3eV$. Presence of a third terminal gives rise two types of local and non-local coefficients. Except for G_{LL} , the rest conductances show two Fano-like resonances. One can explain this feature based on the quantum interferences effect caused by different pathways of electrons due to the coupling of the third terminal to the Benzene molecule.

It is also believed that a sharp change in the conductance characteristic would lead to a sharp enhancement of thermopower (Seebeck). For two terminal case at low temperature this can be easily explained by Mott's formula $S = -\frac{\pi^2}{3} \frac{k_B^2 T}{e} \frac{\sigma'(\mu)}{\sigma}$. It can be seen that for the three terminal set up a great enhancement takes place for S_{PP} and S_{PL} .

Now, we consider temperature influence on the figure of merit particularly focusing on the efficiency at maximum power. For a two-terminal configuration, we use the well known efficiency at maximum power formula as $\eta^\parallel(P_{max}) = \frac{\eta_c^\parallel}{2} \frac{ZT}{2+ZT}$, where $ZT = \frac{GS^2T}{K}$ is the two-terminal figure of merit. For the three terminal case, we use Eq.(8). Indeed, in a numerical approach, after fixing parameters, we monitor the heat currents J_α^Q with

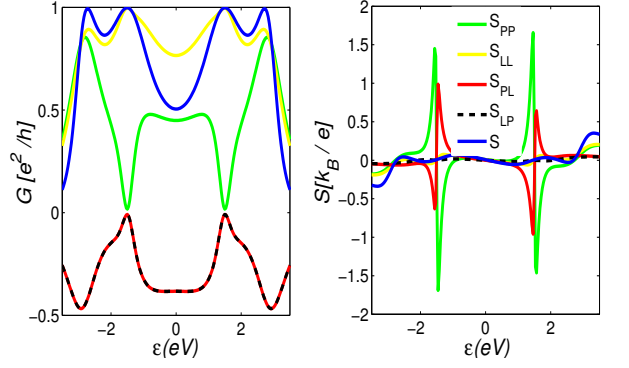


FIG. 2: (Color online) Different thermopowers $S_{\alpha\beta}$, ($\alpha = L, P$), with local S_{LL} (pink line), S_{PP} (green line) and non-local S_{LP} (dashed black line), S_{PL} (red line) are plotted in left panel, and corresponding electrical conductances $G_{\alpha\beta}$ are plotted in right panel. The blue line shows the results of the two-terminal case. The temperature difference is fixed by $M = 0.1$ and couplings are considered in a symmetric way as $\gamma_P = \gamma_L = \gamma_R = 2.5eV$.

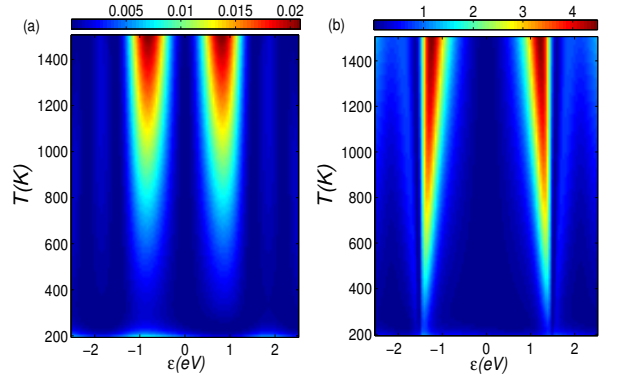


FIG. 3: (Color online) Density plots of figures of merit ZT for a two-terminal configuration (left panel) and $Z_L T$ for configuration-(a) (right panel) as a function of level position and temperature. Parameters are the same as Fig. 2

($\alpha = L, R, P$) then regarding the positivity of heat current, the corresponding efficiency and finally, the figure of merit is calculated. We use the same parameters as Fig. 2. Left and right panels of Fig. 3 show the density plot of the figure of merit as a function of on-site energy ε and temperature for a two-terminal configuration and configuration-(a). One can see that the value of $Z_L T$ for the three terminal case (right panel) is significantly enhanced in the vicinity of $\varepsilon = \pm 1$ and reaches a value $\simeq 4.5$.

We also consider the thermoelectric properties of configuration-(b) (see Fig. 1). Among many choices, as the preceding paragraph, we focus on the figure of merit. Fig. 4, by tuning $M = 0.1$ while the temperature difference between reservoirs L and P is fixed. Again with monitoring the following $J_L^Q > 0$ and $J_{R,P}^Q < 0$ conditions the data for $\eta(P_{max})$ are collected. In this configuration,

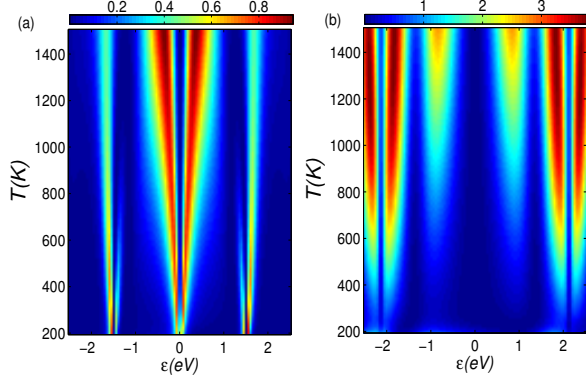


FIG. 4: (Color online) Same as Fig. 3, but for configuration-(b)

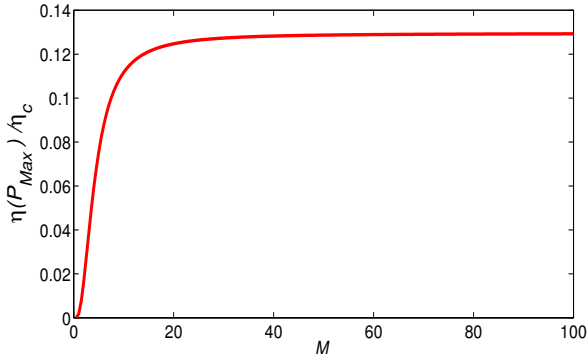


FIG. 5: (Color online) Efficiency at maximum output power normalized over Carnot efficiency as a function of M for configuration-(a). For $0 \leq M < 0.57$ the system absorbs heat only from reservoir L ($J_L^Q > 0$, $J_{R,P}^Q < 0$); for $0.57 \leq M < 18.5$ the system absorbs heat from reservoirs L and P ($J_R^Q < 0$, $J_{L,P}^Q > 0$); and finally, for $18.5 \leq M \leq 100$ the system absorbs heat only from reservoir P ($J_P^Q > 0$, $J_{R,L}^Q < 0$).

the two terminal case shows a big value $\simeq 0.9$ for ZT about $\varepsilon = 0$ which pertains to the quantum interference effect discussed later. Likewise, for three-terminal model a great enhancement up to $\simeq 4$ near $\varepsilon = \pm 2$ is observed.

In Fig. 5, the efficiency at maximum output power normalized over Carnot efficiency $\eta(\mathbf{P}_{max})/\eta_c$ is plotted as a function of M for configuration-(a). Energy is fixed at $\varepsilon = 1.43eV$. The chemical potentials ($\delta\mu_{L,P}$) are chosen to guarantee maximum output power, i.e., fixing the generalized forces ($X_{L,P}^T$) to optimize the output power \mathbf{P} . For $0 \leq M < 0.57$ the system absorbs heat only from reservoir L ($J_L^Q > 0$, $J_{R,P}^Q < 0$); while for $0.57 \leq M < 18.5$ the system absorbs heat from reservoirs L and P ($J_R^Q < 0$, $J_{L,P}^Q > 0$); and finally, for $18.5 \leq M \leq 100$ the system absorbs heat only from reservoir P ($J_P^Q > 0$, $J_{R,L}^Q < 0$). Note that, to follow the linear response regime in our work, we set $\delta T_L = 10^{-3}T$ for $M \leq 2$ and $\delta T_P = 10^{-3}T$ for $M > 2$. As can be seen from the Fig. 5, the efficiency at maximum power

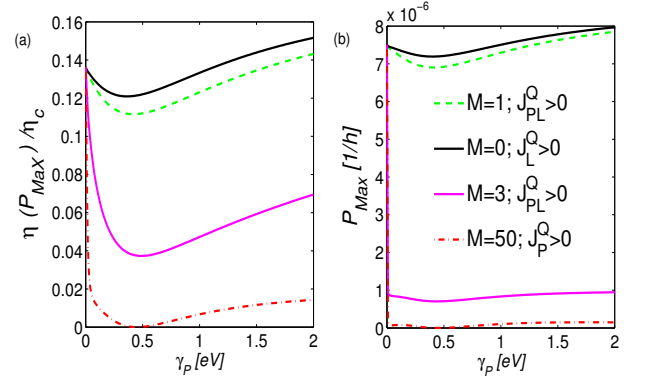


FIG. 6: (Color online) Efficiency at maximum output power, normalized over the Carnot limit for configuration-(a) as a function of γ_P (left panel). Maximum output power extracted by the thermal machine, as a function of γ_P (right panel). Different temperature ratio $M = 0$ (dotted black line), $M = 1(3)$ (solid green(pink) line), and $M = 50$ (dashed red line) corresponding to $J_L^Q > 0, J_{P,R}^Q < 0$, $J_R^Q < 0, J_{P,R}^Q > 0$, and $J_P^Q > 0, J_{L,R}^Q < 0$ are considered. Other parameters are set as $T = 300K$, $\varepsilon = 1.56eV$, and $\gamma_L = \gamma_R = 0.1eV$.

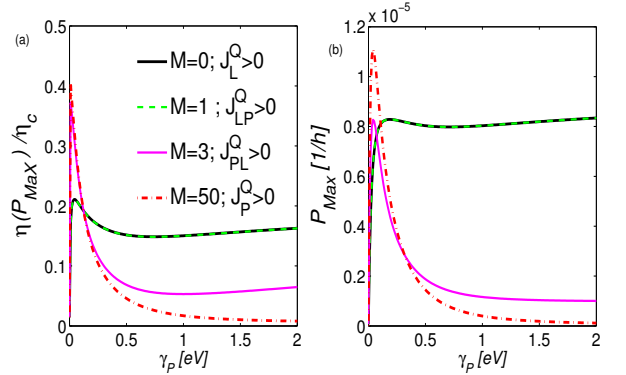


FIG. 7: (Color online) Same as Fig. 6, but for configuration-(b)

increases dramatically and then stabilizes, raising from almost zero at $M = 0$ to reach a saturation value 0.12 about $M = 30$. It shows that for the strong and symmetric coupling case ($\gamma_P = \gamma_L = \gamma_R = 2.5eV$), the efficiency at maximum output power for the system under consideration cannot exceed 0.12, even if high values of M are set.

Let's focus on how the efficiency at maximum output power and the maximum output power evolve when the system is driven from a two-terminal to a three-terminal configuration, that is by tuning γ_P . The two terminal system corresponds to $\gamma_P = 0$ and the third terminal is switched on by increasing γ_P . For simplicity, the coupling strengths of terminals L and R are taken equal to γ , whereas the coupling strength to terminal P is considered as γ_P .

Fig.6 drawn for configuration-(a), we set $M = 0$ (dotted-black line), $M = 1, (3)$ (green, (pink) line)

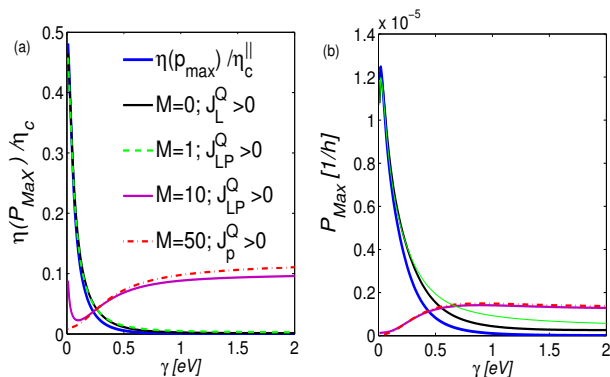


FIG. 8: (Color online) $\eta(\mathbf{P}_{max})/\eta_c$ (left panel) and \mathbf{P}_{max} (right panel) for two-terminal model (blue line) and for configuration-(a) as a function of $\gamma_L = \gamma_R = \gamma$. $M = 0, M = 1$ if $\delta T_L = 10^{-3}T$ and $M = 10, M = 50$ if $\delta T_P = 10^{-3}T$. Other parameters are set as $T = 300K$, $\varepsilon = 1.56eV$, and $\gamma_P = 2.0eV$.

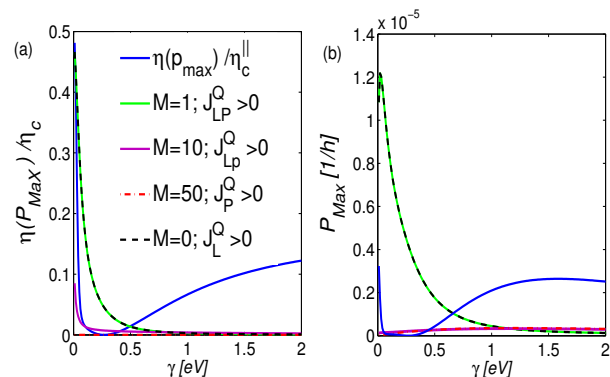


FIG. 9: (Color online) Same as Fig.8, but for configuration-(b)

and $M = 50$ (dashed-red line) leading to $\eta_L(\mathbf{P}_{max})/\eta_c$ when the system absorbs heat only from contact L , $\eta_{LP}(\mathbf{P}_{max})/\eta_c$ when the system absorbs heat from contacts L and P , and $\eta_P(\mathbf{P}_{max})/\eta_c$ when the system absorbs heat only from contact P , respectively. It is seen that increasing the coupling γ_P strength leads to improvement of the performance. As shown in Fig. 6 both $\eta_L(\mathbf{P}_{max})$ and \mathbf{P}_{max} increase for all values of M when $\gamma_P \geq 0.5eV$.

In Fig. 7, we show results for the same quantities but for configuration-(b). In particular, it can be seen that for parameters $M = 0$ and $M = 1$ the efficiency at maximum output power (left panel) and maximum output power (right panel) increase at small couplings and then fall down steadily, while for $M = 50$ and $M = 3$ these quantities increase at small couplings γ_P and then drop sharply, reaching almost zero at $\gamma_P = 2eV$ for $M = 50$.

Next, in Fig. 8 we show results for $\eta(\mathbf{P}_{max})/\eta_c$ (left panel) and \mathbf{P}_{max} (right panel) for the case of two-terminal and configuration-(a) with parameters $M = 0(M = 1)$ if $\delta T_L = 10^{-3}T$ and $M = 10(M = 50)$ if $\delta T_P = 10^{-3}T$, as a function of $\gamma_L = \gamma_R = \gamma$ for two

values of $\gamma_P = 0$ and $\gamma_P = 2.0eV$. Note that, for parameters $M = 1, (M = 0)$ the efficiency coincides with that of a two-terminal system. Results show that the efficiency at maximum output power for $M = 0$ and $M = 1$ tend to $\eta(\mathbf{P}_{max})/\eta_c = 0.5$ and $\eta(\mathbf{P}_{max})/\eta_c = 0$ in the limit $\gamma \rightarrow 0$ and $\gamma \rightarrow \infty$, respectively, while the trends for $M = 10$ and $M = 50$ are opposite. For these values of M , the efficiency at maximum output power tends to zero in the limit $\gamma \rightarrow 0$ and reaches about 0.15 for strong coupling limit. The maximum output power saturating the Carnot bound $\eta(\mathbf{P}_{max})/\eta_c = 0.5$ in the limit $\gamma \rightarrow 0$ for two-terminal case which is due to delta shaped transmission function resulting in the divergence of the figure of merit ZT . The same two contact strong energy dependence of electron transport explains the three-terminal results. Indeed, the three-terminal model is one way to achieve a narrow energy-dependent transport. In the right panel of Fig. 8, the maximum output power show the same trend as efficiency at maximum power for all parameters of M .

In Fig. 9, we show the same quantities as in Fig. 8, but for configuration-(b). As can be seen from the figure at small coupling γ for $M = 1(M = 0)$, is greater than the two-terminal setup. In contrast to the two-terminal case which shows a sharp decrease to zero and then a revival feature versus coupling change, the three-terminal model for $M = 0, 1$ show an exponential decrease. For other M options, we have not seen eminent trend compared to the two-terminal model, while for configuration-(a) in Fig. 8 at strong coupling regime these M options showed finite value for the efficiency at maximum output power and maximum output power.

Before concluding, we comment on the realization of our funding. A great challenge in building molecule-based electronic devices is making reliable molecular junctions and controlling the electrical current through the junctions. The mechanically controllable break junction technique⁵⁶ with integrated nanoscale thermocouples⁵⁷ which is accessible by the current experimental apparatus would one possible way to test the theoretical results in this work.

IV. SUMMARY

In summary, with the help of the Landauer-Buttiker formalism and within time-reversal symmetry, the linear response thermoelectric properties through a Benzene molecule coupled to three non-magnetic electrodes is studied. We consider the two well-known para and meta configurations and added a third terminal in the ortho position. We focus on the temperature difference and coupling strength to find a setup which drives the system to a condition which can show better efficiency than the conventional two-terminal junction. By introducing temperature difference parameter M between terminals and tuning its value, we found cases where the efficiency at maximum output power and maximum output power

of three-terminal configuration exceed the typical two-terminal model. Particularly, under $M = 0.1$ the figure of merit is dramatically influenced by the temperature for both configurations considered.

Appendix A: Linear response and Onsager reciprocal relations

The four well-known Onsager matrix \mathcal{L} elements, the electrical conductance G , the Peltier coefficient Π , the thermal conductance K and the Seebeck coefficient S under certain limitations gauge the transport properties of the system. The case for multi-terminal setup is extended to the introduction of nonlocal coefficients, which describe the influence of bias driven between two terminals on the another terminal. By assuming linear regime, namely small thermodynamic forces, the relationship between fluxes and forces can be as ($J = \mathcal{L}X$)

$$\begin{bmatrix} J_L^N \\ J_L^Q \\ J_P^N \\ J_P^Q \end{bmatrix} = \begin{bmatrix} \mathcal{L}_{11} & \mathcal{L}_{12} & \mathcal{L}_{13} & \mathcal{L}_{14} \\ \mathcal{L}_{21} & \mathcal{L}_{22} & \mathcal{L}_{23} & \mathcal{L}_{24} \\ \mathcal{L}_{31} & \mathcal{L}_{32} & \mathcal{L}_{33} & \mathcal{L}_{34} \\ \mathcal{L}_{41} & \mathcal{L}_{42} & \mathcal{L}_{43} & \mathcal{L}_{44} \end{bmatrix} \begin{bmatrix} X_L^\mu \\ X_L^T \\ X_P^\mu \\ X_P^T \end{bmatrix} \quad (\text{A1})$$

with time-reversal invariance of the equations of motion, Onsager found fundamental relations, known as Onsager reciprocal relations for the cross coefficients of the Onsager matrix $\mathcal{L}_{ij} = \mathcal{L}_{ji}$. Due to the positivity of the entropy production rate, such a matrix has to be semi-positive definite (i.e. $\mathcal{L} \geq 0$) and that it can be used to introduce a two-terminal configuration that connect electrode L with electrode R by setting $L_{j3} = L_{j4} = L_{3j} = L_{4j} = 0$ for $j = 1, 2, 3, 4$.

For a two-terminal system, the Seebeck coefficient S relates the voltage difference δV between the terminals to their temperature difference δT with an open circuit condition (zero charge current), the electrical conductance (G) describes the electric current dependence on the voltage differences between the two-terminal when two terminals have the same temperature, the thermal conductance (K) describes the heat current dependence on the temperature difference δT under the assumption that no net charge current is flowing through the system, and the Peltier effect (Π) relates the heat current to the charge current under isothermal condition. An extension to the multi-terminal scenario is achieved by introducing the matrices of elements

$$\begin{aligned} G_{ij} &= \left[\frac{e^2 J_i^N}{\delta \mu_j} \right]_{\delta T_k=0 \forall k} ; & K_{ij} &= \left[\frac{J_i^Q}{\delta T_j} \right]_{J_k^N=0 \forall k} \\ S_{ij} &= - \left[\frac{\delta \mu_i}{e \delta T_j} \right]_{J_k=0 \forall k} ; & \Pi_{ij} &= \left[\frac{J_i^Q}{e J_j^N} \right]_{\delta T_k=0 \forall k} \end{aligned} \quad (\text{A2})$$

with local ($i = j$) and non-local ($i \neq j$) coefficients, e being the electron charge.

Appendix B: Scattering approach in linear response regime: The Onsager coefficients

The heat and particles currents through a non-interacting conductor can be described by the multi-terminal Landauer-Buttiker approach⁵³. Assuming that all non-coherent processes, phase breaking and dissipative, happen in the terminals, the charge and heat currents from terminal L (reservoir) are given by^{54,55}

$$\begin{aligned} J_L^N &= \frac{1}{h} \int dE \sum_{j \neq L} [\mathcal{T}_{jL}(E) f_L(E) - \mathcal{T}_{Lj}(E) f_j(E)] \\ J_L^Q &= \frac{1}{h} \int dE (E - \mu_L) \sum_{j \neq L} [\mathcal{T}_{jL}(E) f_L(E) - \mathcal{T}_{Lj}(E) f_j(E)] \end{aligned} \quad (\text{B1})$$

where $f_j(E) = [\exp[(E - \mu_j)/k_B T_j] + 1]^{-1}$ is the Fermi function and \mathcal{T}_{ij} is the transmission probability from terminal L to terminal j . Analogous expressions can be defined for J_P^N and J_P^Q , provided the terminal L is substituted by P .

For a three-terminal configuration, one choose the electrode R as the reference ($\mu_R = \mu = 0, T_R = T$). As in the previous sections, one set $\mu_{L,P} = \mu + \delta \mu_{L,P}$, $T_{L,P} = T + \delta T_{L,P}$. The Onsager coefficients \mathcal{L}_{ij} can be obtained from the linear response expansion ($J = \mathcal{L}X$) of the currents J_i^N and J_i^Q ($i = L, P$);

$$\begin{aligned} \mathcal{L}_{11} &= -\frac{T}{h} \int_{-\infty}^{\infty} \left[f'(E) \sum_{\gamma \neq L} \mathcal{T}_{L\gamma}(E) \right] dE \\ \mathcal{L}_{12} &= -\frac{T}{h} \int_{-\infty}^{\infty} \left[f'(E) (E - \mu) \sum_{\gamma \neq L} \mathcal{T}_{L\gamma}(E) \right] dE = \mathcal{L}_{21} \\ \mathcal{L}_{22} &= -\frac{T}{h} \int_{-\infty}^{\infty} \left[f'(E) (E - \mu)^2 \sum_{\gamma \neq L} \mathcal{T}_{L\gamma}(E) \right] dE \\ \mathcal{L}_{13} &= \frac{T}{h} \int_{-\infty}^{\infty} \left[f'(E) \mathcal{T}_{LP}(E) \right] dE = \mathcal{L}_{31} \\ \mathcal{L}_{14} &= \frac{T}{h} \int_{-\infty}^{\infty} \left[f'(E) (E - \mu) \mathcal{T}_{LP}(E) \right] dE = \mathcal{L}_{41} \\ \mathcal{L}_{24} &= \frac{T}{h} \int_{-\infty}^{\infty} \left[f'(E) (E - \mu)^2 \mathcal{T}_{LP}(E) \right] dE = \mathcal{L}_{42} \\ \mathcal{L}_{23} &= \frac{T}{h} \int_{-\infty}^{\infty} \left[f'(E) (E - \mu) \mathcal{T}_{LP}(E) \right] dE = \mathcal{L}_{32} \\ \mathcal{L}_{33} &= -\frac{T}{h} \int_{-\infty}^{\infty} \left[f'(E) \sum_{\gamma \neq P} \mathcal{T}_{P\gamma}(E) \right] dE \\ \mathcal{L}_{34} &= -\frac{T}{h} \int_{-\infty}^{\infty} \left[f'(E) (E - \mu) \sum_{\gamma \neq P} \mathcal{T}_{P\gamma}(E) \right] dE = \mathcal{L}_{43} \\ \mathcal{L}_{44} &= -\frac{T}{h} \int_{-\infty}^{\infty} \left[f'(E) (E - \mu)^2 \sum_{\gamma \neq P} \mathcal{T}_{P\gamma}(E) \right] dE \end{aligned} \quad (\text{B2})$$

where $f'(E)$ is the Fermi-Dirac distribution derivative with respect to the energy and T is the temperature.

As mentioned before, within the time reversal symmetry

$$\mathcal{L}_{ij} = \mathcal{L}_{ji}.$$

- ¹ Majumdar, A. Thermoelectricity in Semiconductor Nanostructures. *Science*, **2004**, 303, 777
- ² Dresselhaus, M. S.; Chen, G.; Tang, M. Y.; Yang, R. G.; Lee, H.; Wang, D. Z.; Ren, Z. F.; Fleurial, J. P.; Gogna, P. New Directions for Low-Dimensional Thermoelectric Materials. *Advanced Materials*, **2004**, 19, 1043
- ³ Snyder, G. J.; Toberer, E. S. Complex Thermoelectric Materials. *Nat Mater*, **2008**, 7, 105
- ⁴ Shakouri, A. Recent Developments in Semiconductor Thermoelectric Physics and Materials. *Annual Review of Materials Research*, **2001**, 41, 399
- ⁵ Vahedi, J.; Barimani, F. Spin and Charge Thermopower Effects in the Ferromagnetic Graphene Junction. *Journal of Applied Physics*, **2016**, 120, 084303
- ⁶ Jacquet, P. A. ThermoElectric Transport Properties of a Chain of Quantum Dots with Self-Consistent Reservoirs. *Journal of Statistical Physics*, **2009**, 709
- ⁷ Entin-Wohlman, O.; Imry, Y.; Aharony, A. Three-Terminal Thermoelectric Transport Through a Molecular Junction. *Phys. Rev. B*, **2010**, 82, 115314.
- ⁸ Entin-Wohlman, O.; Aharony, A. Three-terminal thermoelectric transport under broken time-reversal symmetry. *Phys. Rev. B*, **2012**, 85, 085401
- ⁹ Jiang, J. H.; Entin-Wohlman, O.; Imry, Y. Thermoelectric Three-Terminal Hopping Transport Through One-Dimensional Nanosystems. *Phys. Rev. B*, **2012**, 85, 075412
- ¹⁰ Jiang, J. H.; Entin-Wohlman, O.; Imry, Y. Hopping Thermoelectric Transport in Finite Systems: Boundary Effects. *Phys. Rev. B*, **2013**, 87, 205420
- ¹¹ Saito, K.; Benenti, G.; Casati, G.; Prosen, T. Thermopower with Broken Time-Reversal Symmetry. *Phys. Rev. B*, **2011**, 84, 201306
- ¹² M. Horvat, and T. Prosen, Railway Switch Transport Model. *Phys. Rev. E*, **2012**, 86, 052102
- ¹³ Balachandran, V.; Benenti, G.; Casati, G. Efficiency of Three-Terminal Thermoelectric Transport Under Broken Time-Reversal Symmetry. *Phys. Rev. B*, **2013**, 87, 165419
- ¹⁴ Sánchez, R.; Büttiker, M. Optimal Energy Quanta to Current Conversion. *Phys. Rev. B*, **2011**, 83, 085428
- ¹⁵ Sánchez, D.; Serra, L. Thermoelectric Transport of Mesoscopic Conductors Coupled to Voltage and Thermal Probes. *Phys. Rev. B*, **2011**, 84, 201307
- ¹⁶ Sothmann, B.; Büttiker, M. Magnon-Driven Quantum-Dot Heat Engine. *Europhysics Letters*, **2012**, 99, 27001
- ¹⁷ Brandner, K.; Saito, K.; Seifert, U. Strong Bounds on Onsager Coefficients and Efficiency for Three-Terminal Thermoelectric Transport in a Magnetic Field. *Phys. Rev. Lett.* **2103**, 110, 070603
- ¹⁸ Brandner, K.; Seifert, U. Multi-Terminal Thermoelectric Transport in a Magnetic Field: Bounds on Onsager Coefficients and Efficiency. *New Journal of Physics*, **2013**, 15, 105003
- ¹⁹ Sothmann, B.; Sánchez, R.; Jordan, A. N.; Büttiker, M. Rectification of Thermal Fluctuations in a Chaotic Cavity Heat Engine. *Phys. Rev. B*, **2012**, 85, 205301
- ²⁰ Mazza, F.; Valentini, S.; Bosisio, R.; Benenti, G.; Giovannetti, V.; Fazio, F.; Taddei, F. Separation of heat and charge currents for boosted thermoelectric conversion, *Phys. Rev. B*, **2015**, 91, 245435
- ²¹ Mahan, G. D.; Sofo, J. O. The Best Thermoelectric. *PNAS*, **1996** 93, 7436
- ²² Muhonen, J. T.; Meschke, M.; Pekola, J. Micrometre-Scale Refrigerators. *Reports on Progress in Physics*, **2012**, 75, 046501
- ²³ Sothmann, B.; Sánchez, R.; Jordan, A. N. Thermoelectric Energy Harvesting with Quantum Dots. *Nanotechnology*, **2015**, 26, 032001
- ²⁴ Benenti, G.; Casati, G.; Prosen, T.; Saito, K. Fundamental Aspects of Steady-State Conversion of Heat to Work at the Nanoscale. *Physics Reports*, **2017** 694, 1
- ²⁵ Duarte, N. B.; Mahan, G. D.; Tadigadapa, S. Thermopower Enhancement in Nanowires via Junction Effects. *Nano Letters*, **2009**, 9, 617
- ²⁶ Heremans, J. P.; Jovovic, V.; Toberer, E. S.; Saramat, A.; Kurosaki, K.; Charoenphakdee, A.; Yamanaka, S.; Snyder, G. J. Enhancement of Thermoelectric Efficiency in PbTe by Distortion of the Electronic Density of States. *Science*, **2008**, 9, 554
- ²⁷ Vo, T. M.; Williamson, A. J.; Lordi, V.; Galli, G. Atomistic Design of Thermoelectric Properties of Silicon Nanowires. *Nano Letters*, **2008**, 8, 1111
- ²⁸ Machon, P.; Eschrig, M.; Belzig, W. Giant Thermoelectric Effects in a Proximity-Coupled Superconductor/Ferromagnet Device. *New Journal of Physics*, **2014**, 16, 073002
- ²⁹ Zebarjadi, M.; Esfarjani, K.; Dresselhaus, M. S.; Ren, Z. F.; Chen, G. Perspectives on Thermoelectrics: From Fundamentals to Device Applications. *Energy Environ. Sci.* **2012**, 5, 5147
- ³⁰ Mazza, F.; Bosisio, R.; Benenti, G.; Giovannetti, V.; Fazio R.; Taddei, F. Thermoelectric Efficiency of Three-Terminal Quantum Thermal Machine. *New Journal of Physics*, **2014**, 16, 085001
- ³¹ Thierschmann, H.; Sánchez, R.; Sothmann, B.; Arnold, F.; Heyn, C.; Hansen, W.; Buhmann, H.; Molenkamp, L. W. Three-Terminal Energy Harvester with Coupled Quantum Dots. *Nat Nano*, **2015**, 10, 854
- ³² Liu, J.; Sun, Q. F.; Xie, X. C. Enhancement of the Thermoelectric Figure of Merit in a Quantum Dot Due to the Coulomb Blockade Effect. *Phys. Rev. B*, **2010**, 81, 245323
- ³³ Michalek, G.; Urbaniak, M.; Bulka, B. R.; Domanski, T.; Wysokinski, K. I. Local and Nonlocal Thermopower in Three-Terminal Nanostructures. *Phys. Rev. B*, **2016**, 93, 235440
- ³⁴ Erdman, P. A.; Mazza, F.; Bosisio, R.; Benenti, G.; Fazio, R.; Taddei, F. Thermoelectric Properties of an Interacting Quantum Dot Based Heat Engine. *Phys. Rev. B*, **2017**, 95, 245432
- ³⁵ Aviram, A.; Ratner, M. A. Molecular Rectifiers. *Chem. Phys. Lett.* **1974**, 29, 277
- ³⁶ Aviram, A.; Ratner, M. A. Electron Transport in Molecular Wire Junctions. *Science*, **2003**, 300, 1384
- ³⁷ Nozaki, D.; Toher, C. The Influence of Linkers on Quantum Interference: A Linker Theorem. *J. Phys. Chem. C*, **2017**, 121, 114451
- ³⁸ Vahedi, J.; Sartipi, Z. Effects of Quantum Interference on the Electron Transport in the Semiconductor/Benzene/Semiconductor Junction. *Molecular Physics*, **2015**, 113, 1422

- ³⁹ Sartip, Z.; Vahedi, J. Shot Noise of Charge and Spin Current of a Quantum Dot Coupled to Semiconductor Electrodes. *J. Phys. Chem. A*, **2015**, 119, 10399
- ⁴⁰ Reddy, P.; Jang, S. Y.; Segalman, R. A.; Majumdar, A. Thermoelectricity in Molecular Junctions. *Science*, **2007**, 315, 1568
- ⁴¹ Dubi, Y.; Ventra, M. D. Colloquium: Heat Flow and Thermoelectricity in Atomic and Molecular Junctions. *Rev. Mod. Phys.*, **2011**, 83, 131
- ⁴² Rincon, J.; Hallberg, K.; Aligia, A. A.; Ramasesha, R. Quantum Interference in Coherent Molecular Conductance. *Phys. Rev. Lett.* **2009**, 103, 266807
- ⁴³ Bergfield, J. P.; Solis, M. A.; Stafford, C. A. Giant Thermoelectric Effect from Transmission Supernodes. *ACS Nano*, **2010**, 4, 5314
- ⁴⁴ Fano, U. Effects of Configuration Interaction on Intensities and Phase Shifts. *Phys. Rev.* **1951**, 124, 1866
- ⁴⁵ Finch, C. M.; García Suárez, V. M.; Lambert, C. J. Giant Thermopower and Figure of Merit in Single-Molecule Devices. *Phys. Rev. B*, **2009**, 79, 03340
- ⁴⁶ García-Suárez, V. M.; Ferradás, R.; Ferrer, J. Impact of Fano and Breit-Wigner Resonances in the Thermoelectric Properties of Nanoscale Junctions. *Phys. Rev. B*, **2013**, 88, 235417
- ⁴⁷ Nakanishi, T.; Kato, T. Thermopower of a Quantum Dot in a Coherent Regime. *J. Phys. Soc. Jpn.* **2007**, 76, 034715
- ⁴⁸ Trocha, P.; Barnaś, J. Large Enhancement of Thermoelectric Effects in a Double Quantum Dot System Due to Interference and Coulomb Correlation Phenomena. *Phys. Rev. B*, **2012**, 85, 085408
- ⁴⁹ Gamez-Silva, G.; Avalos-Ovando, O.; LadrAn de Guevara, M. L.; Orellana, P. A. Enhancement of Thermoelectric Efficiency and Violation of the Wiedemann-Franz Law Due to Fano Effect. *Journal of Applied Physics* **2012**, 111, 053704
- ⁵⁰ Van den Broeck, C. Thermodynamic Efficiency at Maximum Power. *Phys. Rev. Lett.* **2005**, 95, 190602
- ⁵¹ H. B. Callen, *Thermodynamics and an Introduction to Thermostatistics* (John Wiley & Sons, New York, 1985).
- ⁵² de Groot, S. R.; Mazur, P. *Non-Equilibrium Thermodynamics* (Dover, New York, 1984).
- ⁵³ Buttiker, M. Coherent and Sequential Tunneling in Series Barriers. *IBM. J. Res. Dev.* **1988**, 32, 63-75.
- ⁵⁴ Imry, Y. *Introduction to Mesoscopic Physics* (Oxford University Press, 1997).
- ⁵⁵ Datta, S. *Electronic Transport in Mesoscopic Systems*, (Cambridge University Press, 1995).
- ⁵⁶ Xiand, D.; Jeong, H.; Kim, D.; Lee, T.; Cheng, Y.; Wang, Q. Three-Terminal Single-Molecule Junctions Formed by Controllable Break Junctions with Side Gating. *Nano Lett.* **2013**, 13, 2809?2813
- ⁵⁷ Lee, E.; Kim, K.; Jeong, W.; Zotti, L.A.; Pauly, F.; Cuevas, J. C.; Reddy, P. Heat dissipation in atomic-scale junctions. *Nature*. **2013**, 498, 209?212